New halloysite-supported bio-based acidic ionic liquid as an efficient catalyst for conversion of fructose to 5-hydroxymethylfurfural: A combined experimental and computational studies

Samahe Sadjadi [a,*], Mohammad Fahimizadeh [b], Naeimeh Bahri-Laleh [a,c], Md Bin Yeamin [d,e], Peng Yuan [b], Albert Poater [d,*]

[a] Iran Polymer and Petrochemical Institute, PO Box 14975-112, Tehran, Iran
[b] School of Environmental Science and Engineering, Guangdong University of Technology, Guangzhou 510006, China
[c] Institute for Sustainability with Knotted Chiral Meta Matter (WPI-SKCM²), Hiroshima University, Hiroshima 739-8526, Japan
[d] Institut de Química Computacional i Catàlisi and Departament de Química, Universitat de Girona, c/ Mª Aurèlia Capmany 69, Girona 17003, Catalonia, Spain
[e] Departament de Química Física i Inorgànica, Universitat Rovira i Virgili, Tarragona, Spain

ABSTRACT

In an effort to design a bio-based catalyst with enough acidic strength to promote the conversion of fructose to 5-hydroxymethylfurfural, a series of halloysite clay-supported acidic ionic liquids were considered as potential candidates. The catalysts could be synthesized from reaction of Cl-functionalized halloysite with histidine, histamine, adenine and tryptophan, followed by treatment with chlorosulfuric acid. Predictive computational studies were performed and approved the superior activity of the histidine-based catalyst. In addition, the computational studies aimed to identify the optimal catalyst using Density Functional Theory (DFT) calculations and other characterization techniques, particularly non covalent interactions plots. Acknowledged by computational results, histidine based catalyst was prepared, characterized and its catalytic activity and recyclability were appraised for the synthesis of 5-hydroxymethylfurfural from fructose as a bio-based starting material. The reaction conditions were optimized and it was revealed that using 30 wt% catalyst, the desired product could be achieved at 100 °C within 1 h. Notably, the catalyst exhibited high recyclability and efficiently promoted the reaction of other mono-saccharides as well.

1. Introduction

The pressing need for sustainable energy solutions and environmental preservation has prompted a shift from conventional fossil fuels, to renewable resources [1,2]. Biomass, in particular, has attracted significant attention for its versatility, being utilized not only in biofuel production [1,3,4], but also in the synthesis of various chemicals and solvents [5]. Biofuels are categorized into four generations based on input feedstock and production processes, with the first two being extensively developed in large-scale, while the last two generations are in lab-scale. Recently, furanic biofuels from non-edible lignocellulosic biomass have gained traction due to their high energy density and cost-effectiveness [6,7,8]. To produce furanic biofuels like 2,5-dimethylfuran (DMF) [9], bio-based starting materials must be first converted to platform compounds, which then tolerate other chemical transformations, such as hydrodeoxygenation to form furanic biofuels. One of the most important platform compounds is 5-hydroxymethylfurfural (HMF) [10,11,12], which is widely used [13,14,15], for the synthesis of various chemicals, including polymers, and solvents, such as levulinic acid, 2,5-furandicarboxylic acid, and 2,5-bis(ethoxymethyl) furan [14,16]. Production of HMF is achieved through acid-catalyzed conversion of saccharides [17], such as fructose under relatively mild reaction conditions [18]. In detail, fructose is a ketohexose, a six-carbon sugar with a ketone group. In aqueous solutions, fructose predominantly exists in its furanose form, which is a five-membered ring structure. This conformation makes fructose more reactive for dehydration reactions compared to glucose, which favors the six-membered pyranose form. The key functional groups in fructose include hydroxyl groups and a ketone group, which play crucial roles in the dehydration process to form HMF. Moreover, HMF production from fructose is also reported

with high efficiency with solid acid catalysts [19]. Actually, according to the literature, the conversion of fructose to HMF is significantly easier than that of other saccharides [20].

Mineral acids such as sulfuric acid and hydrochloric acid are frequently employed in the dehydration of fructose to HMF due to their potent acidity, which effectively facilitates the reaction. However, their use is accompanied by significant drawbacks. These acids often induce side reactions that generate undesired byproducts like levulinic acid and formic acid, which diminish the overall yield of HMF [18]. To address these issues and improve process efficiency, researchers have investigated various alternative catalysts. One first promising category is solid acid catalysts, which encompass materials such as sulfonated resins, zeolites, and metal–organic frameworks (MOFs). These catalysts offer several advantages over traditional mineral acids. Notably, they are reusable, which enhances their economic viability and sustainability. Additionally, solid acids mitigate the corrosion problems commonly associated with mineral acids, thereby prolonging the lifespan of the reaction equipment and reducing maintenance costs. On the other hand, a second alternative category involves the use of ionic liquids (ILs), especially those with acidic functional groups. ILs have demonstrated significant potential in enhancing the dehydration process of fructose to HMF [21]. Their unique properties create an optimal reaction environment that can increase both the selectivity and yield of HMF. ILs' tunable nature allows for the customization of their chemical properties to better suit specific reaction conditions, making them a versatile tool in achieving higher efficiency and reducing byproduct formation. Overall, these alternative catalysts represent significant advancements in the field, offering solutions to the challenges posed by traditional mineral acids and paving the way for more efficient and sustainable production of HMF from fructose. Thus, in this transformation from fructose to HMF, wise choice of acid catalyst and solvent plays the crucial role and determines the selectivity towards HMF [17]. In this regard, the use of heterogeneous catalysts [22,23], such as H-form zeolites [24], which benefit from facile recovery and potentially high recyclability, is advantageous from an economic viewpoint. Moreover, bio-based catalysts can contribute to environmentally friendly process and avoiding the use of hazardous chemicals and solvents during catalyst synthesis [25]. One of the natural compounds, which has been extensively utilized in catalysis is clay, such as halloysite (Hal). Hal is an aluminosilicate clay with general formula of $Al_2(OH)_4Si_2O_5 \cdot 2H_2O$ [26,27,28]. Hal not only benefits from the general features of clays, such as high thermal and mechanical stability, but also exhibits unique features, including cylindrical morphology and opposite electrical charge on its outer and inner layers [29,30,31,32,33,34,35,36], making it an ideal choice as a catalyst support. More interestingly, Hal exhibits acidic properties, and its acidity can be tuned through both physical and chemical modifications [37,38]. Hence, Hal can be considered a bio-based catalyst for acid-catalyzed reactions, such as the conversion of saccharides to HMF. However, our previous work on Hal-based catalysts for the conversion of fructose to HMF highlighted that Hal was not sufficiently acidic to efficiently promote the reaction, necessitating enhancements in its acidity [39]. To address this limitation, we explored various approaches, including supporting heteropolyacids on Hal [38]. Although this significantly improved Hal's acidity and catalytic activity, there were concerns regarding the leaching of heteropolyacid, potentially impacting catalyst recyclability. Additionally, the type of heteropolyacid played a crucial role in the catalyst's performance. As an alternative approach, we investigated chemical modifications of Hal using acidic compounds such as Gum Arabic [40], *k*-carrageenan [25], bio-based Lewis acids [41] and ILs [37], which are organic salts [42,43,44,45,46,47] comprising organic cations and organic/inorganic anions.

Acidic ILs are very promising catalysts. However, their homogeneous nature renders them less attractive from both economic and environmental standpoints. It has been proven that aromatic ILs are more efficient than aliphatic ones [37].

Unfortunately, aromatic ILs are costly and not environmentally benign. To address these issues and create a heterogeneous bio-based catalyst for HMF production, we used Hal, an acidic natural clay, as a support and covalently grafted a bio-based acidic IL onto it. This approach heterogenized the IL and improved the acidity of Hal-IL. We considered natural compounds such as histidine, histamine, adenine, and tryptophan, which contain heterocyclic rings that can be converted to carbocation moieties in ILs, to synthesize the bio-based IL. In other words, instead of using commercial imidazole or similar compounds to form ILs, we focused on biological compounds with fewer environmental concerns.

We evaluated a series of Hal-supported bio-based ILs derived from histidine, histamine, adenine, and tryptophan through computational investigations to identify the most promising catalyst for fructose-to-HMF conversion [48]. Subsequently, following the principles of predictive catalysis [49,50], the chosen catalyst was subsequently synthesized, characterized, and comprehensively assessed for its catalytic performance in the target reaction.

2. Experimental (see SI for further details)

2.1. Materials and devices

Materials such as Hal, (3-chloropropyl)triethoxysilane, CPTES, histidine, chlorosulfuric acid, dimethylsulfoxide, DMSO, and various sugars were obtained from Sigma-Aldrich and used without purification. Catalyst formation was verified using Fourier transform infrared (FT-IR), X-ray diffraction (XRD), temperature programmed desorption of ammonia (NH3-TPD), thermogravimetric analysis (TGA), Scanning electron microscopy (SEM), and energy-dispersive X-ray spectroscopy (EDS) techniques. HMF production was quantitatively analyzed using Gas chromatography (GC) and High-performance liquid chromatography (HPLC). The details of these instruments are presented in SI.

3. Procedures

3.1. Synthesis of Hal-IL

To prepare Hal-IL, Hal was treated with CPTES, histidine, and chlorosulfuric acid. First, Hal (4 g) was suspended in toluene (40 mL), sonicated for 10 min (power of 150 W), and mixed with CPTES (4 mL) under reflux at 110 °C overnight. The resulting Hal-Cl was filtered via centrifugation (8000 rpm), rinsed with toluene (80 mL), and dried at 60 °C. Hal-Cl (3 g) was then mixed with an aqueous histidine solution (2 g in 30 mL) under N_2 for 48 h at 60 °C, forming Hal-H. Finally, Hal-H was suspended in CH_2Cl_2 (40 mL), reacted with chlorosulfuric acid (1 mL), mixed for 24 h, and dried at 60 °C to obtain Hal-IL (Fig. 1).

3.2. Conversion of fructose to HMF

To convert fructose to HMF, fructose (0.2 g) was dissolved in DMSO (7 mL) and reacted with Hal-IL (0.06 g) at 100 °C for 1 h. After cooling to ambient temperature, Hal-IL was separated by centrifugation (8000 rpm), rinsed with DMSO (70 mL), and dried at 60 °C. HMF was obtained by adding NaCl-saturated water (10 mL) to the filtrate, forming organic and aqueous phases [40]. The organic phase HMF was collected by rotary evaporation, while the aqueous phase HMF was separated using diethyl ether (36 mL) and distilled. HMF yield was calculated based on initial fructose moles (Eq. 1).

$$HMF\,yield\,(\%) = \frac{Mole\,(HMF)}{Mole(S)} \times 100\% \qquad (1)$$

3.3. Computational details

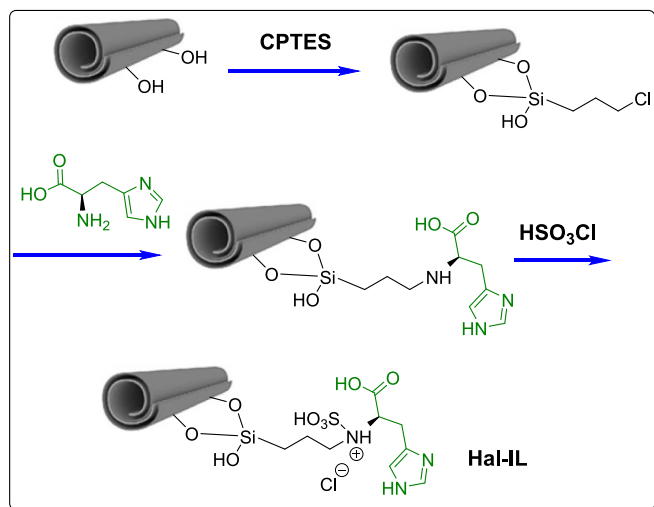The Gaussian 16 package was used for all DFT calculations [51].

Fig. 1. Schematic synthetic route of Hal-IL.

Geometry optimizations employed the BP86 functional [52,53] with Grimme D3 dispersion corrections [54], and the def2SVP basis set [55,56]. Analytical frequency calculations identified stationary points. Single-point energies were calculated using B3LYP [57,58,59] with the def2TZVP basis set [60]. Solvent effects were modeled with the SMD method in DMSO [61].

4. Results and discussion

To shed light on the crystalline structure of Hal-IL, the XRD pattern of Hal-IL was obtained and compared with the pristine Hal. As illustrated in Fig. 2a, characteristic peaks of pristine Hal appeared at $2\theta = 12°$, $19.8°$, $24.7°$, $26.5°$, $35.1°$, $38.2°$, $55.1°$ and $62.4°$ [62,63], which is indicative of the purity of the used Hal. In the XRD pattern of Hal-IL, all characteristic peaks of Hal are distinguished without displacement, underlying that Hal instinct structure was maintained during the chemical treatment and the formed IL did not penetrate within Hal lumen. The only difference between the two recorded patterns was the peak intensity of Hal-IL, which was lower than that of Hal. This observation is in good agreement with the literature and can be ascribed to the grafting of IL on Hal [64].

To further confirm the conjugation of the IL moiety and the

formation of Hal-IL, Fourier Transform Infra Red Spectroscopy (FTIR) spectra of both Hal-IL and pristine Hal were recorded and compared, Fig. 2b. According to the literature [46], the characteristic absorbance bands in Hal appear at 535 cm^{-1} (Al–O–Si vibration), 692 cm^{-1} (stretching vibration of Al–OH), 797 cm^{-1} (symmetric stretching of Si–O–Si), 1051 cm^{-1} (Si–O stretching) and 3693 and 3622 cm^{-1} (inner –OH). In the FTIR spectrum of Hal-IL, the aforementioned absorbance bands are detectable, which is indicative of the stability of Hal in reaction with CPTES, histidine and chlorosulfuric acid. However, the FTIR spectrum of Hal-IL is distinct from that of Hal and some additional bands are observable at 2974 and 1716 cm^{-1}, which are representative of –CH$_2$ and –C=O bands in the IL moiety.

The thermal stability of Hal-IL was explored by recording its thermogram and comparing it with that of pristine Hal. Hal, as a clay mineral exhibits high thermal stability, Fig. 3, and in its thermogram two weight loss steps at ~106 °C and 500 °C are observed as a result of loss of water and dehydroxylation respectively. Thermogram of Hal-IL is different from that of Hal and apart from the weight loss steps due to dehydration and dihydroxylation, an additional one at 300 °C is observable that is attributed to the decomposition of IL moiety. The DTG curve of Hal-IL, Fig. 3, further confirms the results.

Hal-IL morphology was inspected by SEM. As shown in Fig. 4a, Hal cylinders can be detected after the introduction of IL on Hal, underscoring that chemical treatment did not induce a significant morphological change.

Further investigation of the catalyst was conducted by performing EDS and elemental mapping analyses. The results, depicted in Fig. 4b, highlighted the presence of C, O, N, Cl, Si, Al and S elements in the structure of the as-prepared catalyst, which is deemed as a proof for the conjugation of IL moiety on Hal. Additionally, dispersion of the aforesaid elements, Fig. 4c, indicated a homogeneous functionalization of Hal with IL, which is a beneficiary factor for catalysis.

The acidity of Hal-IL was also examined via NH$_3$-TPD analysis and compared with that of pristine Hal. According to the results, Table 1, Hal possesses weak and medium acidic sites and its total acidity was 0.16 mmol/g cat. Upon introduction of IL, the acidity of Hal increased remarkably to 0.55 mmol/g cat and apart from weak and medium acidic sites, strong acidity was also recognized.

Textural properties of Hal-IL, encompassing specific surface areas (S_{BET}) and total pore volume (V_P) were also obtained and compared with those of Hal, Table 2. As tabulated, the specific surface area of Hal decreased upon introduction of IL, implying grafting of IL on the surface of Hal. Similarly, V_P volume decreased from 0.12 cm^3 g^{-1} to 0.11 cm^3
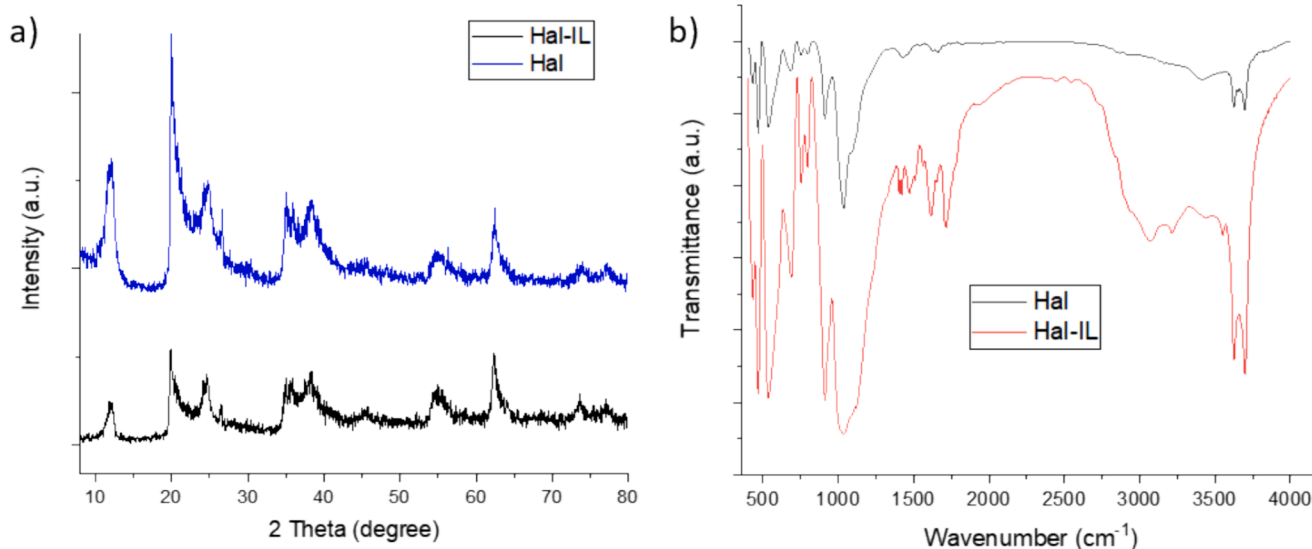

Fig. 2. Comparison of a) XRD patterns and b) FTIR spectra of Hal and Hal-IL.
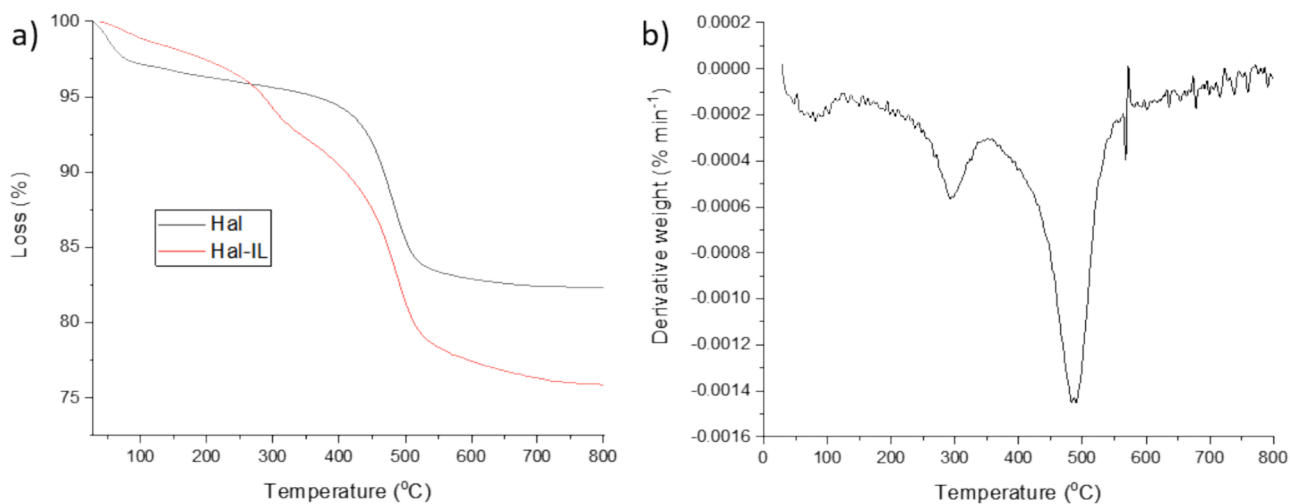
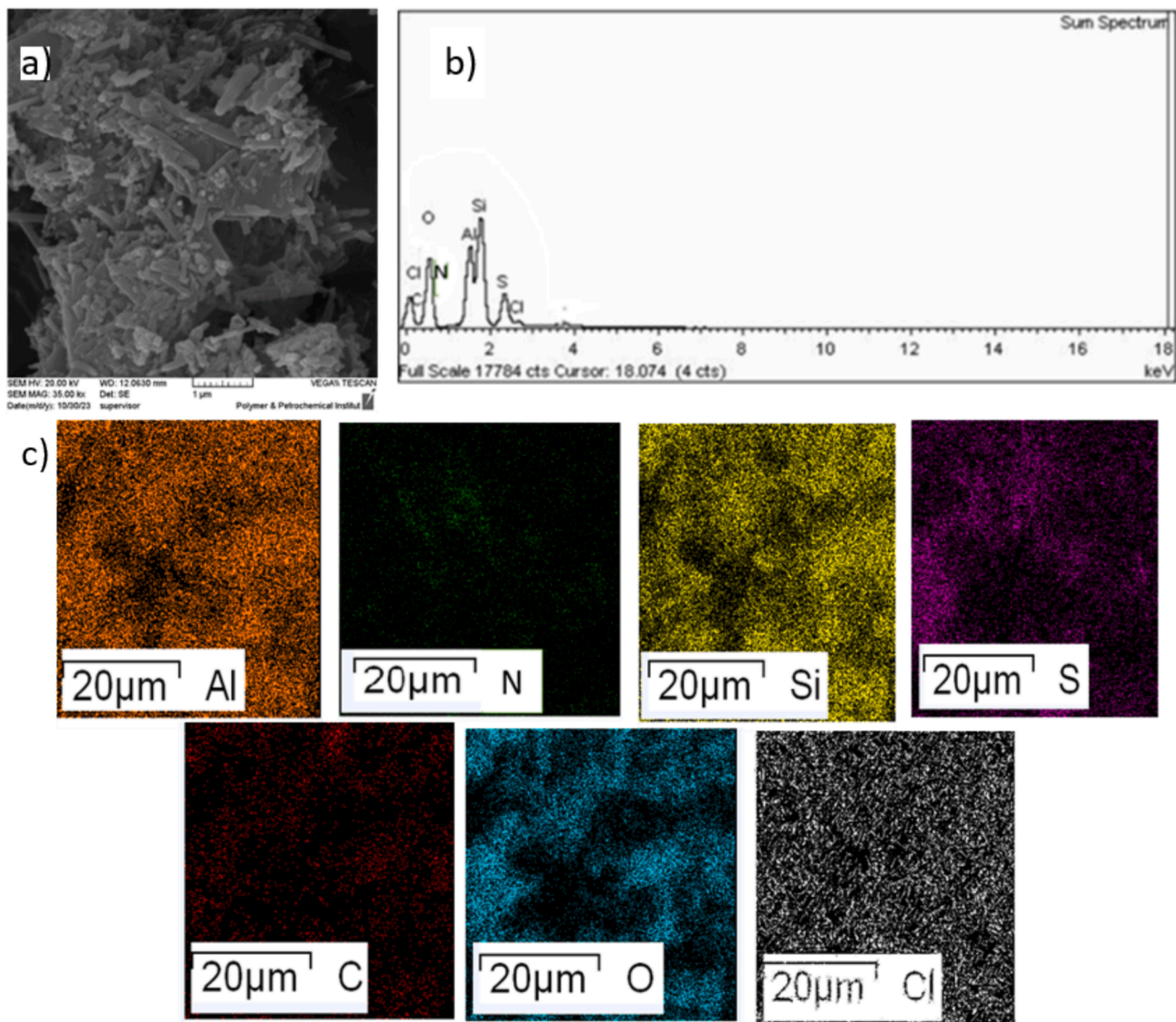**Fig. 3.** a) thermograms of Hal and Hal-IL, b) DTG curve of Hal-IL.

Fig. 4. a) SEM image, b) EDS and c) elemental mapping analyses of the catalyst.

Table 1
NH$_3$−TPD results for acid-treated and pristine Hal.

Catalyst	Weak acidity (100–300 °C)	Medium acidity (300–500 °C)	Strong acidity (above 500 °C)	Total acidity (mmol/g cat)
Hal	0.14	0.02		0.16
Hal-IL	0.1	0.23	0.22	0.55

Table 2
Textural properties of Hal and Hal-IL.

Catalyst	S$_{BET}$ (m^2/g)	V$_P$ (cm^3 g^{-1})
Hal	51	0.12
Hal-IL	43	0.11

g^{-1}.

4.1. Study of catalytic activity of Hal-IL

The conversion of fructose to HMF is a key acid-catalyzed chemical transformation. The main challenge for this reaction is designing a catalyst with high efficiency and selectivity towards HMF. With this aim, Hal, which is a natural clay mineral with instinct acidity, was applied as a catalyst and its acidity was improved by conjugation of a bio-based acidic IL. To appraise the catalytic performance of Hal-IL and achieve the maximum amount of HMF, optimization of the reaction variables, including loading of Hal-IL, reaction temperature and time is imperative. To optimize the reaction temperature, conversion of fructose to HMF was conducted in DMSO using 30 wt% Hal-IL at five different temperatures ranging from 80 to 120 °C. The comparison of the HMF yield, Fig. 5a, underscored that upon increase of the reaction temperature from 80 to 100 °C, HMF yield increased constantly and reached 95 %. Further raising the reaction temperature had the opposite effect and decreased the HMF yield. This observation is aligned with the literature [20] and can be attributed to the possibility of condensation of the produced HMF to humin or other by-products. The effect of the reaction time was appraised by conducting the reaction at 100 °C using 30 wt% Hal-IL and monitoring the progress of the reaction at different time intervals. According to the results, Fig. 5b, upon prolonging the reaction, HMF yield increased and reached its maximum value after 60 min. However, continuing the reaction resulted in a decrease in the HMF yield due to the formation of by-products, mainly humin. To optimize the Hal-IL loading, the target reaction was repeated using different loadings of Hal-IL (10–50 wt%) and the HMF yield of each reaction was measured. As shown in Fig. 5c, increasing the catalyst loading from 10 to 30 wt% effectively improved the HMF yield from 67 to 95 %. Indeed, more active sites can be accessed by increasing the catalyst loading and this problem may lead to the formation of some by-products through further reactions of the formed HMF.
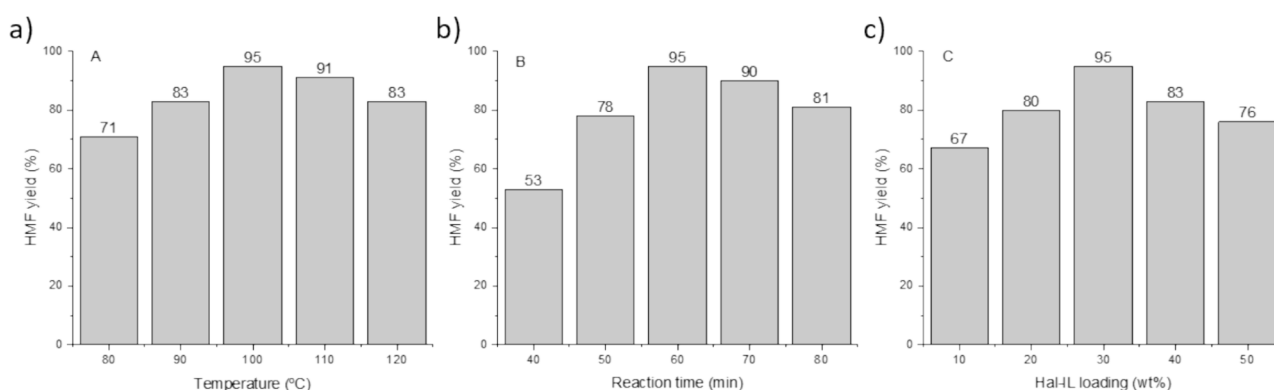
4.2. Recyclability test

As a next part of this study, the recyclability of Hal-IL in the fructose dehydration was appraised. To this aim, the target reaction was performed under optimal conditions and at the end of the reaction the catalyst was recovered by several washings with DMSO and drying at 60 °C. The activity of the recovered Hal-IL for the next run of the reaction was evaluated under exactly the same conditions. The result, Fig. 6a, implied that the loss of the catalytic activity was insignificant (2 %) and HMF with 93 % yield was obtained. Similarly, the recovery and reuse of the catalyst was conducted up to seven consecutive runs and upon each recycling slight loss of activity was observed, which can be due to the coverage of the active sites of Hal-IL by reagent and product. Overall, the recycling test approves that Hal-IL is a recyclable catalyst, which is a promising feature form economic viewpoint. The structural stability of the reused Hal-IL was scrutinized by recording the XRD pattern of the recycled Hal-IL after the seventh reaction run, Fig. 6b. As presented, the XRD pattern of the recycled catalyst also exhibited the characteristic peaks of the fresh Hal-IL, approving the stability of Hal-IL under recycling.

4.3. Generality

Gratifyingly, Hal-IL exhibited high catalytic activity and recyclability for the conversion of fructose, which is a conventional and reactive saccharide. It would be appealing if this catalyst could promote conversion of other saccharides, which are less active. To investigate this issue, performance of Hal-IL for conversion of two monosaccharides, i.e. glucose and galactose, and two disaccharides, sucrose and maltose, was studied under optimum reaction conditions. The results, displayed in Fig. 6c, underlined that conversion of the examined monosaccharides resulted in lower HMF yields compared to fructose, which is due to the necessity of their isomerization to fructose. However, the catalytic activity of Hal-IL for conversion of those substrates was still acceptable and HMF with good yields were obtained for both glucose and galactose. Switching to disaccharides led to the remarkable decrease of HMF yield. This observation is justified by considering the fact that disaccharide conversion required hydrolysis and isomerization steps prior to dehydration.

4.4. Computational studies

To identify the optimal catalyst for the conversion of fructose to HMF, Density Functional Theory (DFT) calculations were conducted. Fig. 7 compares the reaction barriers at the rate-determining state (rds), i.e. transition state (TS) **II-III**, of Hal-supported bio-based ILs derived from histidine, histamine, adenine, and tryptophan, with that of Cl-functionalized halloysite treated with chlorosulfuric acid, which serves as the reference catalyst, truncating the Hal for the sake of clarity.
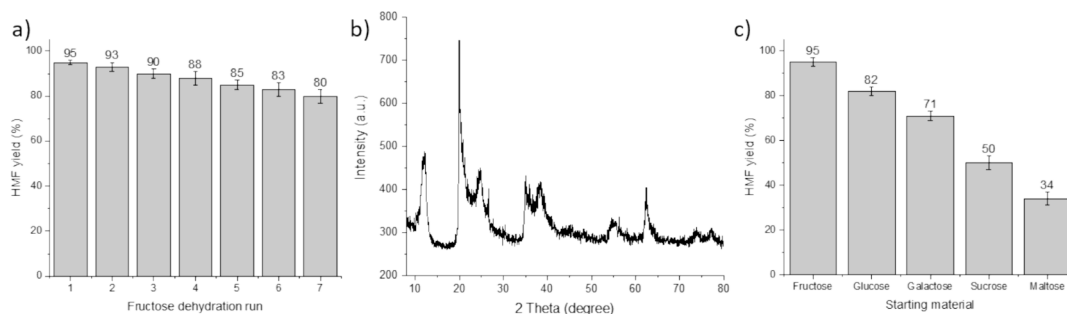

Fig. 5. Investigation of the effects of a) reaction temperature, b) reaction time and c) Hal-IL loading on the HMF yield.

Fig. 6. a) Catalyst recycling results for the dehydration of fructose to HMF under optimal reaction conditions, b) XRD pattern of the recycled catalyst after seven cycles and c) the activity of Hal-IL for conversion of various substrates to HMF.
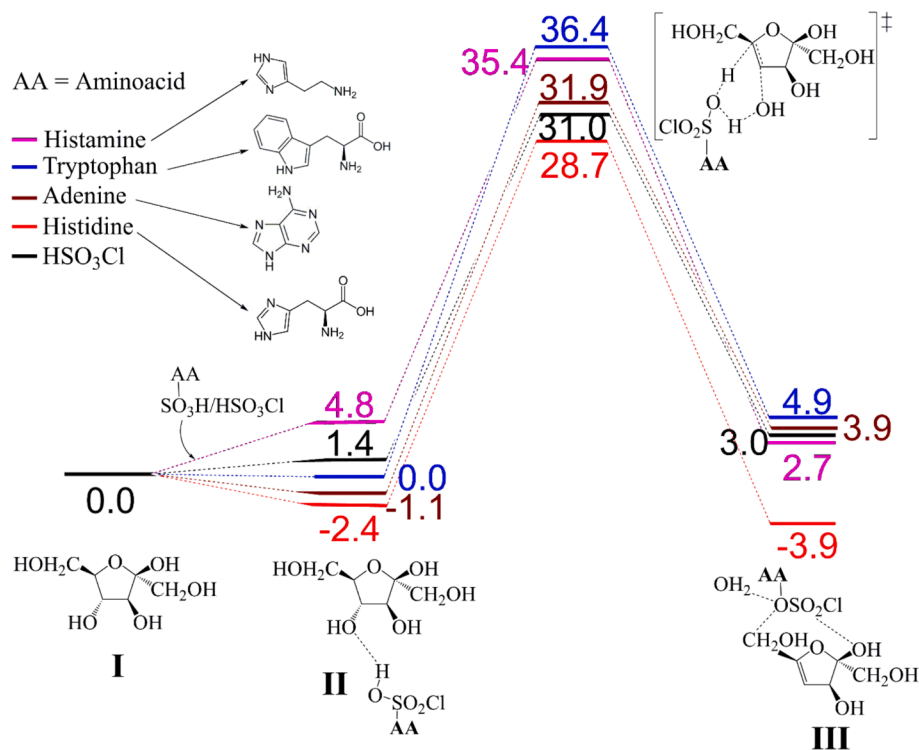

Fig. 7. Comparison of the activation Gibbs energy barriers (in kcal/mol) at the rds of the Cl-functionalized halloysite with histidine, histamine, adenine and tryptophan, at the B3LYPD3/def2TZVP(smd-H2O)//BP86-D3/def2SVP level of theory.

Among these, the histidine-modified catalyst emerged as the preferred bio-based option due to its lowest activation barrier of 31.1 kcal/mol at the rds, which closely approaches the corresponding kinetic cost of the reference catalyst (31.0 kcal/mol), taking into account the rate determining intermediate (rdi) that for histidine and adenine is **II**, whereas the initial **I** for the other three amino acids. Next, with tryptophan, adenine and histamine the kinetics worsen, with values of 36.4, 31.9 and 35.4 kcal/mol, respectively. Thus, tryptophan and histamine showed the worst performance, with the difference between them being relatively minor [65,66]. And next to elucidate the complete reaction mechanism, we compare the mechanism of the histidine-modified catalyst with the reference catalytic system, actually without the histidine. Fig. 8 illustrates the reaction pathway of the reference system, indicating activation barriers of 29.6, 5.4, 7.4, and 0.0 kcal/mol for the four transition steps, respectively, that involve 3 dehydration steps, actually correcting what was stated by some us recently. However, those kinetic costs increase up to 31.0, 6.2, 18.9 and 3.6 kcal/mol bearing the criterium of the corresponding rds. Subsequently, Fig. 8 also depicts the reaction pathway of the histidine-modified catalytic system, highlighting the corresponding activation barriers of 31.1, 8.8, 4.9, and 0.2 kcal/mol for

the respective steps, that translated to the same kinetic costs except for the third that requires 14.7 kcal/mol.

Structurally, there is an asynchrony in the energy barrier among the four amino acids, prompting the need to understand why histidine exhibits a much lower kinetic cost compared to histamine or tryptophan. Firstly, to assess any steric hindrance issues, steric maps by Cavallo and coworkers [67,68] were executed for the rds TS **II-III**, which is determinant, as well as its preceding intermediate, which in most cases is also the rdi. Unexpectedly, there is little correlation between kinetics and the total %V_{Bur} results [69], with TS **II-III**, or rather, with a negligible difference (see Table S1 and Fig. 9) [70]. However, it should be noted that histidine encounters less hindrance compared to the other amino acids, with a total %V_{Bur} value of 45.0 %, and tryptophan at 46.9 %, with histamine (45.3 %) and adenine (46.7 %) in between. In the case of the intermediate **II**, qualitatively similar results are observed, but without a clear definition. In the quadrant analysis, there is some indication that the two most occupied quadrants certify a poorer kinetic behavior by tryptophan and histamine. Nevertheless, compared to single complexes [71,72], or less flexible systems like the active center of proteins [73] or enzymes [68], the maps here fail to capture the complexity of favorable
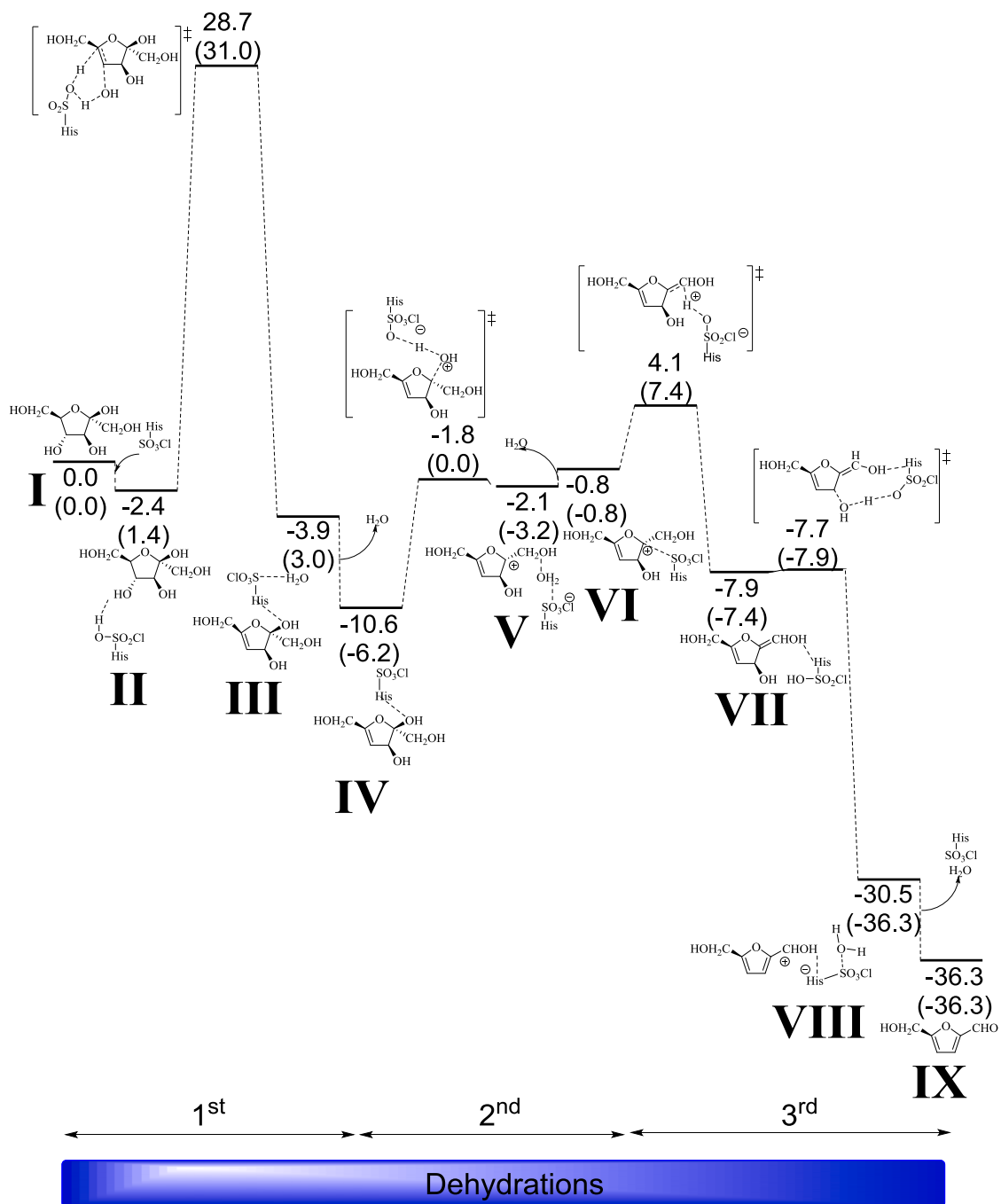
Fig. 8. Reaction pathway of the transformation from fructose (**I**) to HMF (**IX**) with histidine, calculated at the B3LYP-D3/def2TZVP(smd-H$_2$O)//BP86-D3/def2SVP level of theory (relative Gibbs energies in kcal/mol with respect to **I**, in parentheses without histidine).
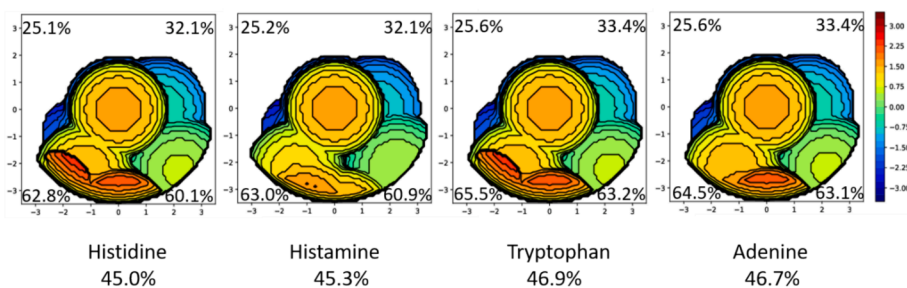

Fig. 9. Steric maps (plane xy) with a radius of 3.5 Å. The centre of the oxygen atom that breaks from the substrate is at the origin, and the carbon atom from which it was bonded on the z axis.

hydrogen bonds [74], which are later addressed within the framework of non-covalent interactions.

Next, simply visualizing TS **II-III** reveals the fundamental role of hydrogen bonds. In general, the formation of a water molecule occurs, indicating a condensation step, and in the TS, the C···O distance of the C–O bond being broken in all cases is approximately 2.4 Å. The hydroxyl attached to sulfur has already donated the proton to oxygen since the O–H distance is close to or even less than the bond length, practically. Importantly, this oxygen, which donates the proton, is stabilized by a hydrogen from a substrate C–H group.

Particularly for histidine (see Fig. 10 and SI for further details), there are two additional H-bonds at 1.808 Å with the substrate, along with another of similar strength at 1.815 Å with the carboxylic group. It

might be thought that the carboxylic group with tryptophan would lead to a similar interpretation, but this is not the case because tryptophan, being positioned further from the substrate, does not allow for any stabilizing H-bonds. Despite having a H-bond at 1.651 Å of much greater strength, it fails to compensate for having only two instead of three as in histidine. Looking at histamine, there are also two H-bonds, but the third one is very weak, being an N–H type between a substrate hydroxyl and an amino acid imidazole group (2.262 Å), poorly oriented even angularly (141.6°). Confirming this, the Mayer Bond Order (MBO) is 0.058 [75], compared to the other two H–bonds mentioned earlier, which are common to all four amino acids, with values of 0.103 and 0.321 [76]. Finally, for adenine, the kinetic cost position is intermediate with MBOs of 0.104, 0.274 for the two general H-bonds, and 0.106 for the specific
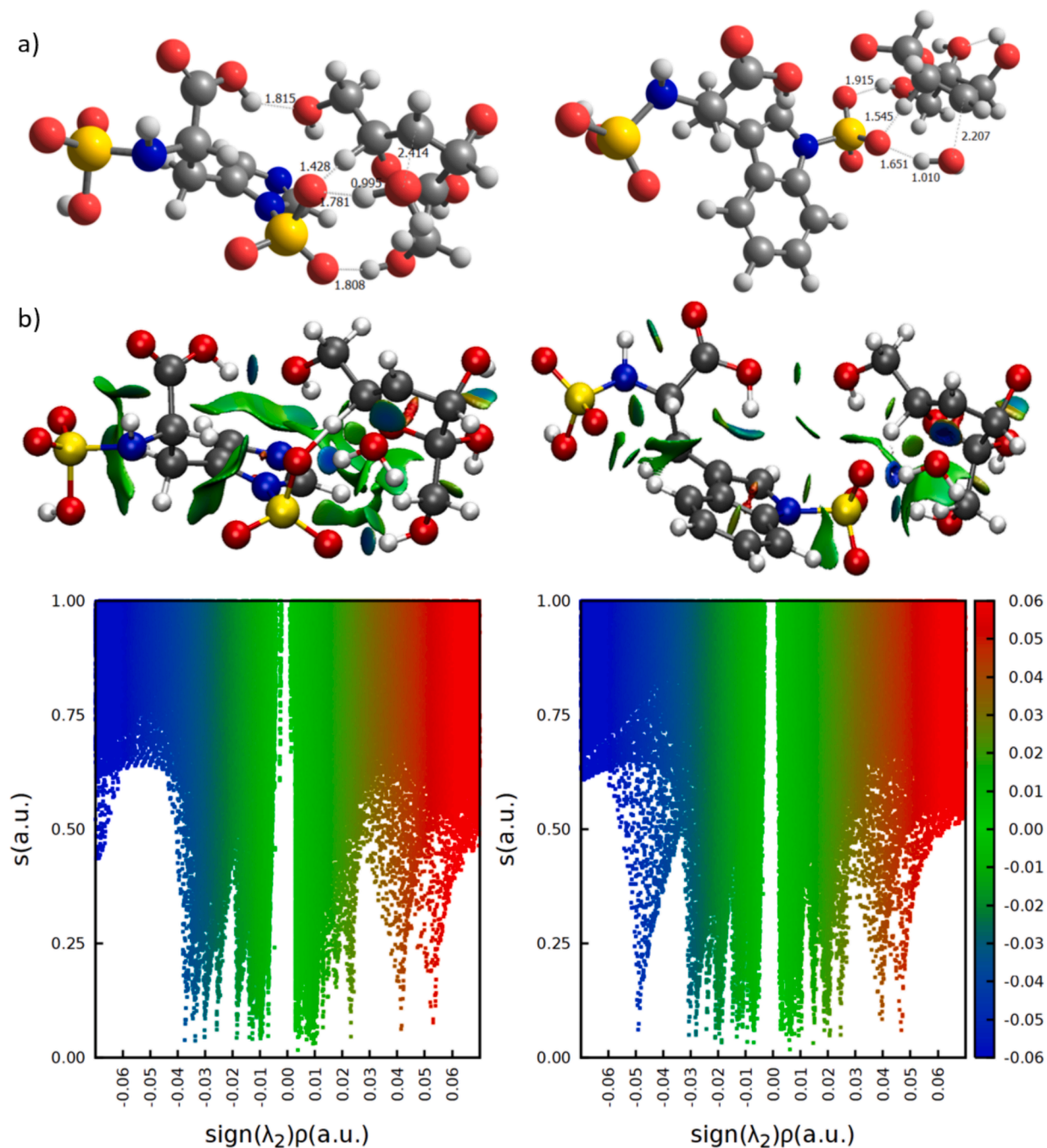

Fig. 10. a) transition state **II-III** (selected distances in Å) and b) 3D (above) and 2D (below) NCI plots of the reduced density gradient (S) vs sign(λ_2)ρ, in a.u, for histidine (left) and tryptophan (right) systems.

O⋯H between a substrate hydroxyl oxygen and an amino acid imidazole CH group. Comparatively, for histidine, the values are 0.341, 0.098, and 0.114, and at the other extreme for tryptophan, 0.267 and 0.098, with no additional H-bonds reported at the MBO level either.

Recognizing the significance of hydrogen bonds, interactions of relatively weak character compared to the prevailing covalent and ionic ones, a non-covalent interactions (NCI) analysis was conducted using NCI plots [77,78]. The 3D profile of TS **II-III** provides straightforward interpretation [79], revealing a much lower contribution from tryptophan compared to histidine (see SI for other species treated, including intermediate **II**) [74,80,81]. In the 2D diagrams [82], there appears to be greater complexity, but understanding that the favorable region lies between 0.00 and −0.04 a.u., it becomes evident that histidine experiences a driving force from the hydrogen bond of the carboxylic group (this becomes even more apparent when compared with histamine and adenine). Conversely, in the region from 0.00 to 0.04 a.u., which represents non-covalent interactions of equally non-favorable nature, the opposite effect is observed. Totally, they all fall within this range of weak van der Waals interactions. Thus, tryptophan exhibits a significantly higher contribution than histidine.

5. Conclusions

In summary, Hal as a natural clay and histidine as an amino acid were applied to form a bio-based heterogeneous acidic catalyst, Hal-IL, to promote the conversion of fructose to HMF. To deepen the study, DFT calculations were exploited to compare the catalytic performance of a series of bio-based Hal-supported ILs, which were obtained from reaction of Hal-Cl with histidine, histamine, adenine and tryptophan, followed by treatment with chlorosulfuric acid. According to the DFT results, IL derived from histidine exhibited the best catalytic performance. Hence, it was selected as a catalyst of the choice and synthesized following the guidelines of predictive catalysis, although we acknowledge that the difference compared to other candidates was not particularly significant. Hydrogen bonds play a crucial role, evident in the NCI analysis, favoring histidine over tryptophan as extreme amino acids due to its higher contribution. The as-prepared catalyst was then characterized and it was found that chemical functionalization of Hal with IL remarkably improved its acidity. Study of the catalytic performance of the catalyst and optimization of the reaction variables also indicated high catalytic activity of the catalyst under mild reaction conditions (HMF was achieved using 30 wt% Hal-IL in DMSO at 100 °C in 1 h). Furthermore, the catalyst was highly recyclable and could catalyze reaction of other mono-saccharides, such as glucose and galactose to furnish HMF in good yields.

CRediT authorship contribution statement

Samahe Sadjadi: Writing – review & editing, Writing – original draft, Investigation, Formal analysis, Conceptualization. **Mohammad Fahimizadeh:** Writing – original draft, Investigation, Formal analysis. **Naeimeh Bahri-Laleh:** Writing – review & editing, Writing – original draft, Supervision, Funding acquisition, Formal analysis, Conceptualization. **Md Bin Yeamin:** Writing – original draft, Visualization, Investigation, Formal analysis. **Peng Yuan:** Writing – review & editing, Writing – original draft, Supervision, Formal analysis. **Albert Poater:** Writing – review & editing, Writing – original draft, Supervision, Investigation, Formal analysis, Conceptualization.

Declaration of competing interest

The authors declare that they have no known competing financial interests or personal relationships that could have appeared to influence the work reported in this paper.

Appendix A. Supplementary data

Supplementary data to this article can be found online at https://doi.org/10.1016/j.molliq.2024.125650.

References

[1] Q. Hou, M. Zhen, L. Liu, Y. Chen, F. Huang, S. Zhang, W. Li, M. Ju, Tin phosphate as a heterogeneous catalyst for efficient dehydration of glucose into 5-hydroxymethylfurfural in ionic liquid, Appl. Catal. B 224 (2019) 183–193.

[2] F.F. Costa, D.T. Oliveira, Y.P. Brito, G.N. Rocha Filho, C.G. Alvarado, A.M. Balu, R. Luque, L.A.S. Nascimento, Lignocellulosics to biofuels: An overview of recent and relevant advances, Curr. Opin. Green Sustain. Chem. 24 (2020) 21–25.

[3] J. Wang, J. Ren, X. Liu, G. Lu, Y. Wang, High yield production and purification of 5-hydroxymethylfurfural, AIChE J. 59 (2013) 2558–2566.

[4] N. Zhu, M. Zhang, G. Qiu, H. Tian, Y. Liu, One-pot synthesis of 5-hydroxymethylfurfural from cellobiose and sucrose using niobium-modified montmorillonite catalysts, Mol. Catal. 532 (2022) 112720.

[5] Y. Ma, S. Qing, L. Wang, N. Islam, S. Guan, Z. Gao, X. Mamat, H. Li, W. Eli, T. Wang, Production of 5-hydroxymethylfurfural from fructose by a thermo-regulated and recyclable Brønsted acidic ionic liquid catalyst, RSC Adv. 5 (2015) 47377–47383.

[6] R. Kourieh, V. Rakic, S. Bennici, A. Auroux, Relation between surface acidity and reactivity in fructose conversion into 5-HMF using tungstated zirconia catalysts, Catal. Commun. 30 (2013) 5–13.

[7] A. Villa, M. Schiavoni, P.F. Fulvio, S.M. Mahurin, S. Dai, R.T. Mayes, G.M. Veith, L. Prati, Phosphorylated mesoporous carbon as effective catalyst for the selective fructose dehydration to HMF, J. Energy Chem. 22 (2013) 305–311.

[8] L. Zhou, R. Liang, Z. Ma, T. Wu, Y. Wu, Conversion of cellulose to HMF in ionic liquid catalyzed by bifunctional ionic liquids, Bioresour. Technol. 129 (2013) 450–455.

[9] H. Son Le, Z. Said, M. Tuan Pham, T. Hieu Le, I. Veza, V. Nhanh Nguyen, B. Deepanraj, L. Huong Nguyen, Production of HMF and DMF biofuel from carbohydrates through catalytic pathways as a sustainable strategy for the future energy sector, Fuel 324 (2022) 124474.

[10] G. Portillo Perez, M.-J. Dumont, Production of HMF in high yield using a low cost and recyclable carbonaceous catalyst, Chem. Eng. J. 382 (2020) 122766.

[11] Y. Zhang, B. Li, W. Guan, Y. Wei, C. Yan, M. Meng, J. Pan, Y. Yan, One-pot synthesis of HMF from carbohydrates over acid-base bi-functional carbonaceous catalyst supported on halloysite nanotubes, Cellulose 27 (2020) 3037–3054.

[12] X. Kong, S.V. Vasudevan, M. Cao, J. Cai, H. Mao, Q. Bu, Microwave-assisted efficient fructose–HMF conversion in water over sulfonated carbon microsphere catalyst, ACS Sustain. Chem. Eng. 9 (2021) 15344–15356.

[13] J. Zhang, Z. Wang, M. Chen, Y. Zhu, Y. Liu, H. He, Y. Cao, X. Bao, N-doped carbon layer-coated Au nanocatalyst for H₂-free conversion of 5-hydroxymethylfurfural to 5-methylfurfural, Chinese, J. Catal. 43 (2022) 2212–2222.

[14] F. Guo, Z. Fang, T.-J. Zhou, Conversion of fructose and glucose into 5-hydroxymethylfurfural with lignin-derived carbonaceous catalyst under microwave irradiation in dimethyl sulfoxide–ionic liquid mixtures, Bioresour. Technol. 112 (2012) 313–318.

[15] D. Papoulis, S. Komarneni, D. Panagiotaras, E. Stathatos, D. Toli, K. C. Chirstoforidis, M. Fernández-García, H. Li, S. Yin, T. Sato, H. Katsuki, Halloysite–TiO2 nanocomposites: Synthesis, characterization and photocatalytic activity, Appl. Catal. B 132–133 (2013) 416–422.

[16] H. Li, Q. Zhang, X. Liu, F. Chang, Y. Zhang, W. Xue, S. Yang, Immobilizing Cr³⁺ with SO₃H-functionalized solid polymeric ionic liquids as efficient and reusable catalysts for selective transformation of carbohydrates into 5-hydroxymethylfurfural, Bioresour. Technol. 144 (2013) 21–27.

[17] F.H. Richter, K. Pupovac, R. Palkovits, F. Schüth, Set of acidic resin catalysts to correlate structure and reactivity in fructose conversion to 5-hydroxymethylfurfural, ACS Catal. 3 (2013) 123–127.

[18] K.I. Galkin, V.P. Ananikov, When will 5-hydroxymethylfurfural, the "Sleeping Giant" of sustainable chemistry, awaken? ChemSusChem 12 (2019) 2976–2982.

[19] K.-I. Shimizu, R. Uozumi, A. Satsuma, Enhanced production of hydroxymethylfurfural from fructose with solid acid catalysts by simple water removal methods, Catal. Commun. 10 (2009) 1849–1853.

[20] B. Agarwal, K. Kailasam, R.S. Sangwan, S. Elumalai, Traversing the history of solid catalysts for heterogeneous synthesis of 5-hydroxymethylfurfural from carbohydrate sugars: A review, Renew. Sust. Energ. Rev. 82 (2018) 2408–2425.

[21] V.T.C. Doan, T.M. Dao, T.A. Huynh, T.T. Nguyen, P.H. Tran, A simple and efficient synthesis of 5-hydroxymethylfurfural from carbohydrates using acidic ionic liquid grafted on silica gel, RSC Adv. 14 (2024) 17480–17490.

[22] Y. Wei, Y. Zhang, Catalytic conversion of mannose to 5-hydroxymethylfurfural promoted by hydrophobic halloysite-based catalyst in biphasic system, Appl. Clay Sci. 254 (2024) 107390.

[23] M. Liu, Y. Zhang, E. Zhu, P. Jin, K. Wang, J. Zhao, C. Li, Y. Yan, Facile synthesis of halloysite nanotubes-supported acidic metal-organic frameworks with tunable acidity for efficient fructose dehydration to 5-hydroxymethylfurfural, ChemistrySelect 2 (2017) 10413–10419.

[24] A. Pande, P. Niphadkar, K. Pandare, V. Bokade, Acid modified H-USY zeolite for efficient catalytic transformation of fructose to 5-hydroxymethyl furfural (biofuel precursor) in methyl isobutyl ketone-water biphasic system, energ, Fuel 32 (2018) 3783–3791.

[25] S. Darvishi, S. Sadjadi, E. Monflier, M.M. Heravi, k-carrageenan nanocomposite as an efficient acidic bio-based catalyst for the synthesis of 5-hydroxymethylfurfural from fructose, J. Mol. Struct. 1296 (2024) 136827.

[26] S. Sadjadi, Halloysite-based hybrids/composites in catalysis, Appl. Clay Sci. 189 (2020) 105537.

[27] L. Lisuzzo, G. Cavallaro, S. Milioto, G. Lazzara, Halloysite nanotubes as nanoreactors for heterogeneous micellar catalysis, J. Colloid Interface Sci. 608 (2022) 424–434.

[28] Z. Asadi, S. Sadjadi, M. Nekoomanesh-Haghighi, S. Posada-Pérez, M. Solà, N. Bahri-Laleh, A. Poate, Lubricant hydrogenation over a functionalized clay-based Pd catalyst: A combined computational and experimental study, Appl. Organomet. Chem. 36 (2022) e6850.

[29] M. Bilal, Z. Jing, Y. Zhao, H. Iqbal, Immobilization of fungal laccase on glutaraldehyde cross-linked chitosan beads and its bio-catalytic potential to degrade bisphenol A, Biocatal. Agric. Biotechnol. 19 (2019) 101174.

[30] V. Vinokurov, A. Stavitskaya, A. Glotov, A. Ostudin, M. Sosna, P. Gushchin, Y. Darrat, Y. Lvov, Halloysite nanotube-based cobalt mesocatalysts for hydrogen production from sodium borohydride, J. Solid State Chem. 268 (2018) 182–189.

[31] R.J. Smith, K.M. Holder, S. Ruiz, W. Hahn, Y. Song, Y.M. Lvov, J.C. Grunlan, Environmentally benign halloysite nanotube multilayer assembly significantly reduces polyurethane flammability, Adv. Funct. Mater. 28 (2018) 1703289.

[32] G. Lazzara, G. Cavallaro, A. Panchal, R. Fakhrullin, A. Stavitskaya, V. Vinokurov, Y. Lvov, An assembly of organic-inorganic composites using halloysite clay nanotubes, Curr. Opin. Colloid Interface Sci. 35 (2018) 42–50.

[33] G. Cavallaro, L. Chiappisi, P. Pasbakhsh, M. Gradzielski, G. Lazzara, A structural comparison of halloysite nanotubes of different origin by small-angle neutron scattering (SANS) and electric birefringence, Appl. Clay Sci. 160 (2018) 71–80.

[34] H. Wang, D. Wu, X. Li, P. Huo, Ce doping TiO₂/halloysite nanotubes photocatalyst for enhanced electrons transfer and photocatalytic degradation of Tetracycline, J. Mater. Sci.: Mater. Electron. 30 (2019) 19126–19136.

[35] V.A. Vinokurov, A.V. Stavitskaya, E.V. Ivanov, P.A. Gushchin, D.V. Kozlov, A.Y. Kurenkova, P.A. Kolinko, E.A. Kozlova, Y.M. Lvov, Halloysite nanoclay based CdS formulations with high catalytic activity in hydrogen evolution reaction under visible light irradiation, ACS Sustain. Chem. Eng. 5 (2017) 11316–11323.

[36] L. Deng, P. Yuan, D. Liu, P. Du, J. Zhou, Y. Wei, Y. Song, Y. Liu, Effects of calcination and acid treatment on improving benzene adsorption performance of halloysite, Appl. Clay Sci. 181 (2019) 105240.

[37] S. Sadjadi, N. Abedian-Dehaghani, X. Zhong, M.M. Heravi, P. Yuan, Ionic liquid-functionalized halloysite as an efficient catalyst for the production of 5-hydroxymethylfurfural, Appl. Clay Sci. 237 (2023) 106896.

[38] F. Saghandali, M. Kazemeini, S. Sadjadi, Halloysite-supported silicotungstic acid as an efficient catalyst for dehydration of fructose to 5-hydroxymethylfurfural, J. Phys. Chem. Solids 184 (2024) 111697.

[39] S. Sadjadi, S. Yaghoubi, M. Heravi, Acid treatment and chemical modification of halloysite as a dual approach to design a catalyst for synthesis of 5-hydroxymethylfurfural, Appl. Clay Sci. 253 (2024) 107369.

[40] S. Sadjadi, S. Yaghoubi, X. Zhong, P. Yuan, M.M. Heravi, Composite of gum arabic and halloysite as a bio-based acidic catalyst for efficient synthesis of 5-hydroxymthylfurfural, Appl. Clay Sci. 247 (2024) 107197.

[41] S. Yaghoubi, S. Sadjadi, X. Zhong, P. Yuan, M.M. Heravi, Clay-supported bio-based Lewis acid ionic liquid as a potent catalyst for the dehydration of fructose to 5-hydroxymethylfurfural, Sci. Rep. 14 (2024) 82.

[42] N.A.S. Ramli, N.A.S. Amin, Catalytic conversion of carbohydrate biomass in ionic liquids to 5-hydroxymethyl furfural and levulinic acid: A review, Bioenergy Res. 13 (2020) 693–736.

[43] S. Sadjadi, Magnetic (poly) ionic liquids: A promising platform for green chemistry, J. Mol. Liq. 323 (2021) 114994.

[44] Y. Zhang, S. Sun, A review on biodiesel production using basic ionic liquids as catalysts, Ind. Crops Prod. 202 (2023) 117099.

[45] S.K. Singh, A.W. Savoy, Ionic liquids synthesis and applications: An overview, J. Mol. Liq. 297 (2020) 112038.

[46] O. Bartlewicz, I. Dabek, A. Szymanska, H. Maciejewski, Heterogeneous catalysis with the participation of ionic liquids, Catalysts 10 (2020) 1227.

[47] P. McNeice, P.C. Marr, A.C. Marr, Basic ionic liquids for catalysis: the road to greater stability, Catal. Sci. Technol. 11 (2021) 726–741.

[48] Z. Hosseini, M. Kazemeini, S. Sadjadi, S. Pourebrahimi, Silicotungstic acid catalyst supported onto functionalized halloysite nanotubes (HNTs) utilized for the production of 5-hydroxymethylfurfural (5-HMF) from fructose, Mol. Catal. 557 (2024) 113992.

[49] S. Escayola, N. Bahri-Laleh, A. Poater, %V_Bur index and steric maps: from predictive catalysis to machine learning, Chem. Soc. Rev. 53 (2024) 853–882.

[50] R. Monreal-Corona, A. Pla-Quintana, A. Poater, Predictive catalysis: a valuable step towards machine learning, Trends Chem. 5 (2023) 935–946.

[51] Gaussian 16, Revision C.01, M.J. Frisch, G.W. Trucks, H.B. Schlegel, G.E. Scuseria, M.A. Robb, J.R. Cheeseman, G. Scalmani, V. Barone, G.A. Petersson, H. Nakatsuji, X. Li, M. Caricato, A.V. Marenich, J. Bloino, B.G. Janesko, R. Gomperts, B. Mennucci, H.P. Hratchian, J.V. Ortiz, A.F. Izmaylov, J.L. Sonnenberg, D. Williams-Young, F. Ding, F. Lipparini, F. Egidi, J. Goings, B. Peng, A. Petrone, T. Henderson, D. Ranasinghe, V.G. Zakrzewski, J. Gao, N. Rega, G. Zheng, W. Liang, M. Hada, M. Ehara, K. Toyota, R. Fukuda, J. Hasegawa, M. Ishida, T. Nakajima, Y. Honda, O. Kitao, H. Nakai, T. Vreven, K. Throssell, J.A. Montgomery, Jr., J.E. Peralta, F. Ogliaro, M.J. Bearpark, J.J. Heyd, E.N. Brothers, K.N. Kudin, V.N. Staroverov, T.A. Keith, R. Kobayashi, J. Normand, K. Raghavachari, A.P. Rendell, J.C. Burant, S.S. Iyengar, J. Tomasi, M. Cossi, J.M. Millam, M. Klene, C. Adamo, R. Cammi, J.W. Ochterski, R.L. Martin, K. Morokuma, O. Farkas, J.B. Foresman, D.J. Fox, Gaussian, Inc., Wallingford CT, 2016.

[52] A.D. Becke, Density-functional exchange-energy approximation with correct asymptotic behavior, Phys. Rev. A 38 (1988) 3098–3100.

[53] J.P. Perdew, Density-functional approximation for the correlation energy of the inhomogeneous electron gas, Phys. Rev. B 33 (1986) 8822–8824.

[54] S. Grimme, J. Antony, S. Ehrlich, H. Krieg, A consistent and accurate ab initio parametrization of density functional dispersion correction (DFT-D) for the 94 elements H-Pu, J. Chem. Phys. 132 (2010) 154104.

[55] F. Weigend, R. Ahlrichs, Balanced basis sets of split valence, triple zeta valence and quadruple zeta valence quality for H to Rn: design and assessment of accuracy, Phys. Chem. Chem. Phys. 7 (2005) 3297–3305.

[56] F. Weigend, Accurate coulomb-fitting basis sets for H to Rn, Phys. Chem. Chem. Phys. 8 (2006) 1057–1065.

[57] A.D. Becke, A.D. Becke, Density-functional thermochemistry. III. The role of exact exchange, J. Chem. Phys. 98 (1993) 5648–5652.

[58] C. Lee, W. Yang, R.G. Parr, Development of the colle-salvetti correlation-energy formula into a functional of the electron density, Phys. Rev. B 37 (1988) 785–789.

[59] P.J. Stephens, F.J. Devlin, C.F. Chabalowski, M.J. Frisch, Ab initio calculation of vibrational absorption and circular dichroism spectra using density functional force fields, J. Phys. Chem. 98 (1994) 11623–11627.

[60] T.H. Dunning Jr, Gaussian basis sets for use in correlated molecular calculations. I. The atoms boron through neon and hydrogen, J. Chem. Phys. 90 (1989) 1007–1023.

[61] A.V. Marenich, C.J. Cramer, D.G. Truhlar, Universal solvation model based on solute electron density and on a continuum model of the solvent defined by the bulk dielectric constant and atomic surface tensions, J. Phys. Chem. B 113 (2009) 6378–6396.

[62] H. Zhu, M.-L. Du, M.-L. Zou, C.-S. Xu, Y.-Q. Fu, Green synthesis of Au nanoparticles immobilized on halloysite nanotubes for surface-enhanced Raman scattering substrates, Dalton Trans. 41 (2012) 10465–10471.

[63] P. Yuan, P.D. Southon, Z. Liu, M.E.R. Green, J.M. Hook, S.J. Antill, C.J. Kepert, Functionalization of halloysite clay nanotubes by grafting with γ-aminopropyltriethoxysilane, J. Phys. Chem. C 112 (2008) 15742–15751.

[64] S. Sadjadi, M. Akbari, F.G. Kahangi, M.M. Heravi, Acidic polymer containing sulfunic acid and carboxylic acid groups heterogenized with natural clay: A novel metal free and heterogeneous catalyst for acid-catalyzed reactions, Polyhedron 179 (2020) 114375.

[65] R. Monreal-Corona, À. Díaz-Jiménez, A. Roglans, A. Poater, A. Pla-Quintana, Indolizine synthesis through annulation of pyridinium 1,4-thiolates and copper carbenes: A predictive catalysis approach, Adv. Synth. Catal. 2023 (365) (2023) 760–766.

[66] N. Joly, M. Gimferrer, S. Escayola, M. Cendra, S. Coufourier, J.-F. Lohier, Q. Gaignard Gaillard, S. Gaillard, M. Solà, J.-L. Renaud, A. Poater, Enhancement of knölker iron catalysts for imine hydrogenation by predictive catalysis: From calculations to selective experiments, Organometallics 42 (2023) 1784–1792.

[67] L. Falivene, R. Credendino, A. Poater, A. Petta, L. Serra, R. Oliva, V. Scarano, L. Cavallo, SambVca 2. A Web Tool for Analyzing Catalytic Pockets with Topographic Steric Maps, Organometallics 35 (2016) 2286–2293.

[68] L. Falivene, Z. Cao, A. Petta, L. Serra, A. Poater, R. Oliva, V. Scarano, L. Cavallo, Towards the online computer-aided design of catalytic pockets, Nat. Chem. 11 (2019) 872–879.

[69] A. Poater, B. Cosenza, A. Correa, S. Giudice, F. Ragone, V. Scarano, L. Cavallo, SambVca: a web application for the calculation of buried volumes of N-heterocyclic carbene ligands, Eur. J. Inorg. Chem. 2009 (2009) 1759–1766.

[70] J. Bosson, A. Poater, L. Cavallo, S.P. Nolan, Mechanism of racemization of chiral alcohols mediated by 16-electron ruthenium complexes, J. Am. Chem. Soc. 132 (2010) 13146–13149.

[71] A. Poater, F. Ragone, R. Mariz, R. Dorta, L. Cavallo, Comparing the enantioselective power of steric and electrostatic effects in transition-Metal-catalyzed asymmetric synthesis, Chem. Eur. J. 16 (2010) 14348–14353.

[72] R. Mariz, A. Poater, M. Gatti, E. Drinkel, J.J. Bürgi, X. Luan, S. Blumentritt, A. Linden, L. Cavallo, R. Dorta, C2-symmetric chiral disulfoxide ligands in

rhodium-catalyzed 1,4-addition: From ligand synthesis to the enantioselection pathway, Chem. Eur. J. 16 (2010) 14335–14347.

[73] A. Poater, Michael acceptors tuned by the pivotal aromaticity of histidine to block COVID-19 activity, J. Phys. Chem. Lett. 11 (2020) 6262–6265.

[74] M. Tabrizi, S. Sadjadi, G. Pareras, M. Nekoomanesh-Haghighi, N. Bahri-Laleh, A. Poater, Efficient hydro-finishing of polyalfaolefin based lubricants under mild reaction condition using Pd on ligands decorated halloysite, J. Colloid Interface Sci. 581 (2021) 939–953.

[75] I. Mayer, Charge, bond order and valence in the AB initio SCF theory, Chem. Phys. 97 (1983) 270–274.

[76] J. Poater, M. Gimferrer, A. Poater, Covalent and ionic capacity of MOFs to sorb small gas molecules, Inorg. Chem. 57 (2018) 6981–6990.

[77] E.R. Johnson, S. Keinan, P. Mori-Sanchez, J. Contreras-Garcia, A.J. Cohen, W. T. Yang, Revealing noncovalent interactions, J. Am. Chem. Soc. 132 (2010) 6498–6506.

[78] J. Contreras-Garcia, E.R. Johnson, S. Keinan, R. Chaudret, J.P. Piquemal, D. N. Beratan, W.T. Yang, NCIPLOT: a program for plotting non-covalent interaction regions, J. Chem. Theory Comput. 7 (2011) 625–632.

[79] J. Contreras-García, R.A. Boto, F. Izquierdo-Ruiz, I. Reva, T. Woller, M. Alonso, A benchmark for the non-covalent interaction (NCI) index or… is it really all in the geometry? Theor. Chem. Acc. 135 (2016) 242.

[80] S. Yousefi, N. Bahri-Laleh, M. Nekoomanesh, M. Emami, S. Sadjadi, S. A. Mirmohammadi, M. Tomasini, E. Bardají, A. Poater, An efficient initiator system containing $AlCl_3$ and supported ionic-liquid for the synthesis of conventional grade polyisobutylene in mild conditions, J. Mol. Liq. 367 (2022) 120381.

[81] A. Shams, M. Mehdizadeh, H.-R. Teimoury, M. Emami, S.A. Mirmohammadi, S. Sadjadi, E. Bardají, A. Poater, N. Bahri-Laleh, Effect of the pore architecture of ziegler-natta catalyst on its behavior in propylene/1-hexene copolymerization, J. Ind. Eng. Chem. 116 (2022) 359–370.

[82] R. Laplaza, F. Peccati, R.A. Boto, Y. Maday, J. Contreras-García, NCIPLOT and the analysis of noncovalent interactions using the reduced density gradient, Wiley Interdiscip. Rev. Comput. Mol. Sci. 11 (2021) e1497.